nature neuroscience

Similar network activity from disparate circuit parameters

Astrid A Prinz, Dirk Bucher & Eve Marder

It is often assumed that cellular and synaptic properties need to be regulated to specific values to allow a neuronal network to function properly. To determine how tightly neuronal properties and synaptic strengths need to be tuned to produce a given network output, we simulated more than 20 million versions of a three-cell model of the pyloric network of the crustacean stomatogastric ganglion using different combinations of synapse strengths and neuron properties. We found that virtually indistinguishable network activity can arise from widely disparate sets of underlying mechanisms, suggesting that there could be considerable animal-to-animal variability in many of the parameters that control network activity, and that many different combinations of synaptic strengths and intrinsic membrane properties can be consistent with appropriate network performance.

Although common sense tells us that no two brains are identical, a series of experimental strategies has evolved, on the basis of studies into the influence of controlled variables on neuronal or network function, that are designed to remove the influence of the underlying variance in neuronal properties and synaptic strengths. These strategies include averaging or normalizing data and comparing each preparation to its own control before and after a treatment. Successful as these strategies may be, they implicitly assume that variability between preparations or animals is 'experimental noise' rather than an essential characteristic of the nervous system. We used computational models to study this underlying variability in synaptic strengths and neuronal properties in the production of a simple motor pattern. Specifically, we searched for combinations of synaptic strengths and intrinsic properties in three-neuron model networks that produced output patterns within the range of the pyloric rhythms generated by the stomatogastric ganglia of 99 lobsters (*Homarus americanus*).

Here we argue that network output might be more tightly regulated than many of the underlying cellular and synaptic properties. Previous computational work using models of single neurons has shown that similar electrical activity can be achieved with varying combinations of ion channels in the neuron's membrane[1–4]. Experimental measurements of single membrane currents in the same individually identified neurons in different preparations show severalfold ranges in conductance densities[2,3,5]. Together, these data suggest that individual neurons 'tune' themselves to achieve combinations of conductance densities that are consistent with a given target excitability[6–9]. This conceptual framework fits with the compensation that occurs after genetic manipulation of channel-gene expression, as alterations in the expression of one channel may be compensated by changes in the density of one or more other channels[10]. We also argue that compensation may occur at the network level as well: that is, each animal's network has a target activity level, and mechanisms exist that allow each animal to produce a target network performance despite having differing sets of synaptic strengths and intrinsic membrane properties. The present study supports this notion by demonstrating that similar and functional network behavior can result from widely differing combinations of intrinsic and synaptic properties.

RESULTS

The pyloric rhythm of the crustacean stomatogastric ganglion (STG) is an ideal test bed for studies of how network performance depends on the properties of the neurons and synapses within a functional circuit[11]. Unlike many preparations with relatively ill-defined outputs or connectivity, this ganglion has a small number of neurons and a stereotyped motor pattern, making it relatively easy to determine when and how network behavior is influenced by changes in synaptic strength or intrinsic membrane properties[12,13].

The pyloric rhythm is a triphasic motor pattern (**Fig. 1**) generated by a circuit whose connectivity has been characterized[11]. In its simplest form, the pyloric rhythm is produced by a pacemaker kernel consisting of the anterior burster (AB) neuron, which is electrically coupled to two pyloric dilator (PD) neurons, and of two types of follower neurons: a single lateral pyloric (LP) neuron and five to eight pyloric (PY) neurons[11]. The follower neurons receive inhibitory glutamatergic synapses with fast dynamics from the AB neuron, and inhibitory cholinergic synapses with slow dynamics from the PD neurons[14–16]. The LP neuron has an inhibitory glutamatergic synapse that feeds back to the PD neurons[15–17], and the LP neuron has reciprocal inhibitory glutamatergic connections with at least some of the PY neurons[18].

Strategy

For the simulations described here, the electrically coupled AB and PD neurons were lumped into a single bursting AB/PD model

Volen Center and Biology Department, Brandeis University, Mail Stop 013, 415 South Street, Waltham, Massachusetts 02454-9110, USA. Correspondence should be addressed to A.A.P. (prinz@brandeis.edu).

Published online 21 November 2004; doi:10.1038/nn1352

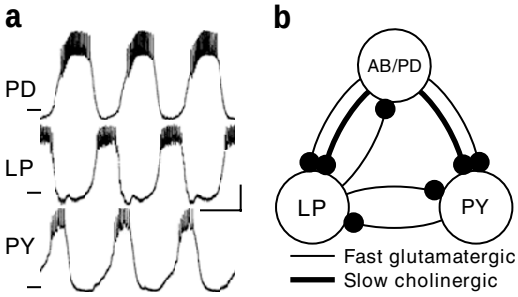

Figure 1 Biological pyloric rhythm and pyloric circuit architecture. (**a**) Pyloric rhythm recorded from *H. americanus* with intracellular electrodes. Scale bars, 1 s and 10 mV; horizontal lines, –60 mV. (**b**) Schematic of a simplified version of underlying circuit. Under control conditions, the pyloric network generates a triphasic rhythm with bursts occurring in the order PD-LP-PY. All synapses in circuit are inhibitory.

neuron, but the fast glutamatergic and slow cholinergic synapses from the AB and PD neurons were simulated separately. All the PY neurons were represented by one model neuron. The individual neuron models had eight membrane conductances (see below) and were complex enough to realistically mimic the dynamics of STG neurons[3,4]. For this work, two other cell types, the ventricular dilator (VD) and inferior cardiac (IC) were not included. These simplifications, along with our use of single-compartment model neurons and simple synaptic dynamics, mean that the model networks studied here are best thought of as semi-realistic models of the biological pyloric circuit that allow us to examine the larger issue of how critical synapse strength is to network dynamics.

The general strategy we employed was to generate a database of more than 20 million model pyloric circuits by (i) independently varying the strengths of the seven synapses in the pyloric circuit model (**Fig. 1**) and (ii) using five or six different versions of each of the neurons in the circuit. Each synapse had one of five or six different strengths: 0 nS, 3 nS, 10 nS, 30 nS, 100 nS and, for synapses onto PY, 1 nS. These cover the entire functionally relevant range of synaptic conductances, from no impact on the postsynaptic cell (0 nS) to 100 nS, which is sufficiently large to effectively clamp the postsynaptic neuron to the synaptic reversal potential for the duration of the synaptic input. To ensure that our conclusions did not result from idiosyncratic properties of any of the model neurons we chose, we used five model AB/PD and LP neurons and six model PY neurons. These model neurons showed activity consistent with the range of behaviors recorded experimentally in these types of neurons when isolated from synaptic inputs from other pyloric network neurons. The model neurons were selected from a previously constructed database of almost 1.7 million model neurons with different combinations of maximal conductances for the currents found in STG neurons[4]. All combinations of synaptic strengths and model neurons were then simulated, resulting in $5^6 \times 6^4 = 20{,}250{,}000$ model circuits with different combinations of synaptic strengths and intrinsic properties.

Properties of the model neurons

The AB/PD model neurons were all intrinsically bursting, and the LP and PY neurons were selected to display ranges of spontaneous activity and postinhibitory rebound (see Methods). One such model neuron, LP #2 (**Fig. 2**), fired tonically in the absence of input. As the strength of the inhibition from AB/PD #3 was increased, it became strong enough to silence LP #2, which then fired on rebound from the inhibition. In response to strong inhibition, the strong rebound burst self-terminated before the next cycle of inhibition. In contrast, LP #5, which was also tonically active in isolation, generated a rebound burst that continued until the start of the next cycle of inhibition.

The responses of two of the PY model neurons to the fast synapse from the AB/PD #3 model neuron are shown (**Fig. 2c**,**d**). PY #4 was tonically active before inhibition, whereas PY #3 was bistable. It was silent before inhibition, but fired indefinitely as a consequence of rebound from the inhibition.

Different types of network output

We first simulated the behavior of 20,250,000 model networks from all of the combinations of neurons and synaptic strengths previously described. We then sorted the resulting network output patterns according to their behaviors (**Fig. 3**). Failure to generate a network output that resembled the crustacean triphasic pyloric rhythm took many forms. We observed rhythms in which one or several cells were silent or fired tonically (**Fig. 3a**,**f**), bursted irregularly (**Fig. 3b**,**g**) or failed to burst in every cycle of the rhythm (**Fig. 3c**,**h**). Some networks generated a triphasic rhythm, but the LP and PY burst order was reversed (**Fig. 3d**,**i**).

In some cases the underlying synapse strengths provided a straightforward explanation for the network output. For example, the networks in **Figure 3d**,**i** had a weak glutamatergic connection from the pacemaker kernel AB/PD to LP and a weak cholinergic connection from AB/PD to PY, but had a strong cholinergic connection from AB/PD to LP and a fairly strong glutamatergic connection from AB/PD to PY. Because the cholinergic synapses are slower than the glutamatergic synapses, this constellation favors a rebound burst in PY before the rebound burst in LP and thus explains the AB/PD-PY-LP burst order of the rhythms generated by the two networks.

In contrast, the cellular and synaptic properties of many of the other networks provided no immediately obvious explanation for the network behavior. Networks illustrated in **Figure 3f–j**, for example, all have the same synaptic strengths but generate very different rhythms because of the different intrinsic properties of the neurons.

Pyloric-like rhythms

To determine how many of the networks in the database could generate a triphasic rhythmic output with the same burst sequence as the biological pyloric rhythm, we identified the start times (peak time of first spike) and end times (peak time of last spike) of all bursts in the output of networks in which all three neurons were bursting periodically. Based on these data, we classified rhythms as 'pyloric-like' if they met the following criteria: in every cycle (defined as the period between one AB/PD burst start and the next), the LP burst began before the start of the PY burst and finished before the end of the PY burst; and the AB/PD burst finished before the start of the LP burst, creating a gap in firing activity (**Fig. 3e**,**j**).

Out of the 20,250,000 networks in the database, 4,047,375 (or 20%) were pyloric-like by these criteria. The networks that generated pyloric-like rhythms were distributed over the full range of sampled synapse strengths for every synapse in the circuit, covering two orders of magnitude of synaptic conductance. Similarly, every one of the $5^2 \times 6 = 150$ possible combinations of cells was represented in the pyloric-like networks, indicating that functional network output can be generated by a wide variety of combinations of synaptic and cellular properties.

Pyloric rhythms

Given that pyloric-like rhythms can be generated by such a wide variety of parameter combinations, we asked whether narrower criteria for the network output would restrict the viable parameter combinations to narrower ranges and thus result in a far smaller number of possible network architectures. To define a physiologically meaningful set of

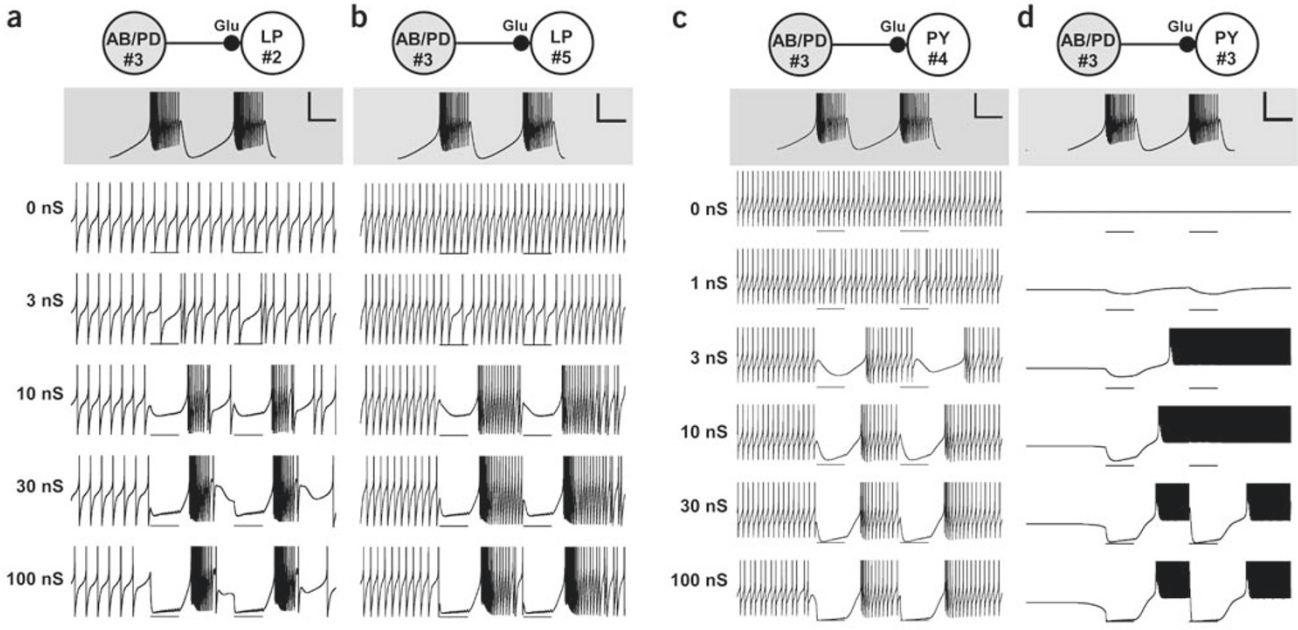

Figure 2 Cellular and synaptic components of the model networks. (**a**–**d**) Shown are examples of LP model neurons (**a**,**b**), and of PY model neurons (**c**,**d**) receiving synaptic inhibition from two bursts of an AB/PD model neuron (top trace in each panel) through synapses of varying strength. The LP models were spikers with a post-inhibitory rebound of (**a**) limited or (**b**) unlimited duration. The PY models were (**c**) spiking, silent, or (**d**) silent but bistable. Synapse strengths ranged from 0 nS (no synapse) to 100 nS (bringing postsynaptic neuron close to synaptic reversal potential of –80 mV). Scale bars, 0.5 s and 20 mV; horizontal lines, –80 mV.

narrow criteria, we used a collection of pyloric-rhythm recordings from 99 lobster (*H. americanus*) preparations under control conditions (D.B., A.A.P. and E.M., unpublished data). We characterized the experimental ranges of 15 salient features of these rhythms by determining the means and standard deviations of the burst period, the burst durations of PD-, LP- and PY-neuron firing, the gaps between the end of the PD neuron burst and the start of the LP neuron burst, and so forth (**Fig. 4a**, **Table 1**; experimental ranges shown as mean ± 2 s.d.).

We determined the values of all 15 measures for the pyloric-like rhythms described above and searched for rhythms for which all 15 measures were in the experimental range (**Fig. 4b**). We call these rhythms and the networks that generate them 'pyloric.' There were 452,516 pyloric rhythms in the database, corresponding to 11% of the pyloric-like networks and to 2.2% of all networks. Even with the narrow criteria for pyloric rhythms, all 150 possible combinations of model neurons were capable of generating a pyloric rhythm.

Similar rhythms from different networks

Pyloric rhythms were generated by networks with very different cellular and synaptic properties (**Fig. 5**; the bursting patterns gener-

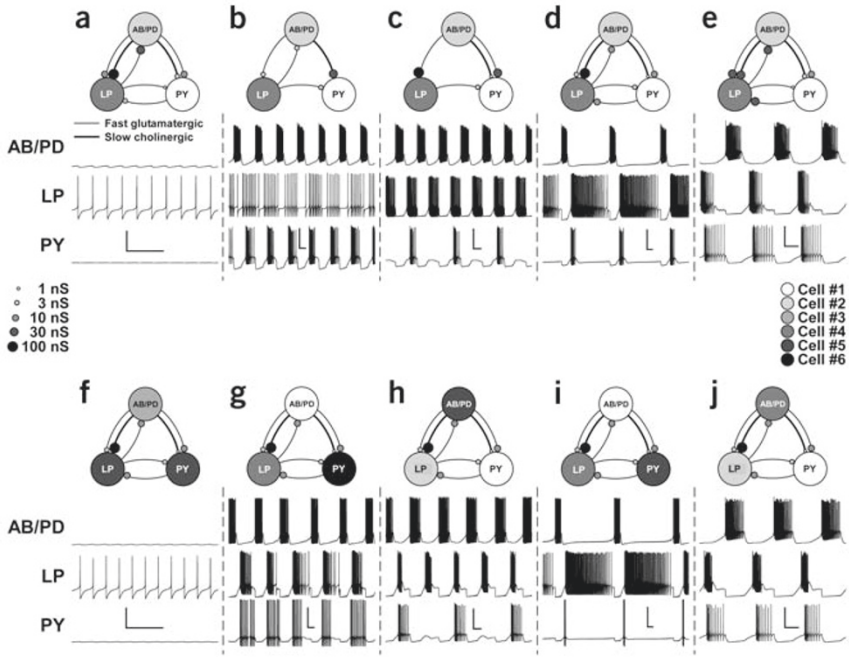

Figure 3 Examples of network outputs. (**a**–**e**) Traces obtained using the same set of model neurons and different synaptic strengths. (**f**–**j**) Traces for different model neurons and the same set of synaptic strengths. (**a**,**f**) LP spiked tonically, AB/PD and PY were silent. (**b**,**g**) Period and burst durations of one or several neurons were variable. (**c**,**h**) Higher-order periodicity. PY burst only once for every two burst cycles in AB/PD and LP. (**d**,**i**) Triphasic burst pattern, but burst order was AB/PD-PY-LP instead of AB/PD-LP-PY. (**e**,**j**) The criteria for pyloric-like rhythm were fulfilled: LP neurons started bursting before PY neurons, LP neurons stopped bursting before PY neurons, an activity gap was present between end of AB/PD bursting and start of LP bursting. Corresponding network configuration indicated at the top of each panel. All scale bars, 50 mV and 0.5 s.

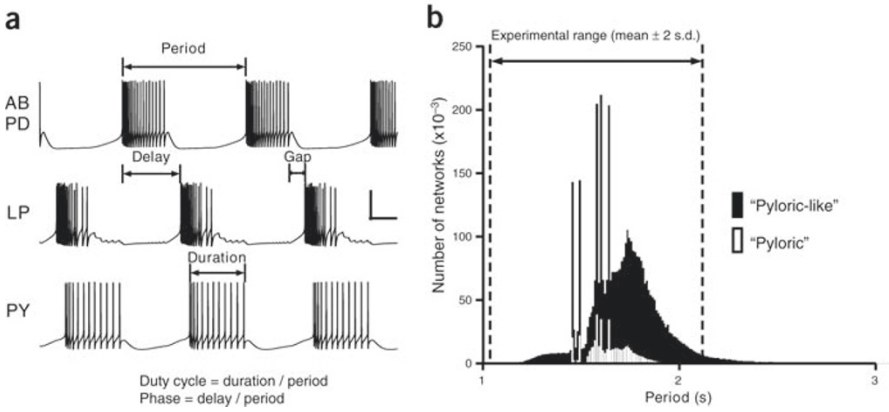

Figure 4 Criteria for pyloric rhythms. (**a**) Simulated networks were classified as pyloric if 15 characteristic features of the rhythmic pattern were within the experimental range. Some of the 15 measures are illustrated here. Scale bars, 0.2 s and 40 mV. (**b**) Experimental cycle period range, 'pyloric-like' cycle period distribution and 'pyloric' cycle period distribution. Most pyloric-like rhythms have cycle periods within the experimental range. Pyloric rhythms have cycle periods equal to or slower than the intrinsic AB/PD pacemaker model periods, which correspond to the five sharp peaks in the distribution.

ated by the two circuits are very similar even though all conductances shown in the figure differ by at least a factor of three). To explore fully the ranges of parameters seen in groups of networks with very similar outputs, we chose three pyloric model networks with burst periods at the lower end, the middle and the upper end of the pyloric period range (**Fig. 6a**). For each of these three model networks, we selected the subset of pyloric circuits that differed by less than 10% from the chosen network in all 15 rhythm characteristics described above. **Figure 6a** shows an example of each of these sets of models, representing the three groups of pyloric rhythms with very narrowly constrained characteristics in the fast ($n = 534$), medium ($n = 633$) and slow ($n = 207$) burst frequency range.

All LP and PY model neurons were represented in the functional pyloric networks and in the fast, medium, and slow network subsets (**Fig. 6b**). In contrast, the fast, medium, and slow networks involved different subsets of the AB/PD model pacemakers, indicating that the burst period of the pyloric network is largely determined by the intrinsic burst period of the pacemaker kernel.

Within the entire set of pyloric networks, every synapse in the circuit covered the full range of tested values, with one exception: the LP-to-PY synapse strength exceeded 3 nS in only 0.1% of the pyloric networks, and was never larger than 30 nS (**Fig. 6c**). The strength of this synapse thus appears to be a critical factor in the generation of the pyloric rhythm. In agreement with our theoretical result, the LP to PY synapse is weak in the biological pyloric circuit[19]. The fact that all other synapse strengths in the pyloric networks varied over the entire functional range confirms that there are many widely differing network configurations that are capable of generating a pyloric rhythm.

Although some of the synapse strength distributions in the fast, medium and slow groups were somewhat narrower than those for the full pyloric set, most synapse strengths in the three groups still varied over the entire functional range. This demonstrates that even very narrowly defined behavior does not necessarily require tight regulation of cellular and synaptic properties of a network.

Table 1 Experimental ranges of salient pyloric rhythm features

Feature	Mean	s.d.	Mean – 2 s.d.	Mean + 2 s.d.
Cycle period (s)	1.509	0.279	0.952	2.067
PD burst duration (s)	0.582	0.133	0.317	0.847
LP burst duration (s)	0.399	0.113	0.172	0.625
PY burst duration (s)	0.530	0.150	0.230	0.830
Gap PD end to LP start (s)	0.221	0.109	0.004	0.439
Gap LP end to PY start (s)	–0.061	0.060	–0.181	0.059
Delay PD start to LP start (s)	0.803	0.169	0.464	1.142
Delay PD start to PY start (s)	1.141	0.216	0.709	1.572
PD duty cycle	0.385	0.040	0.305	0.464
LP duty cycle	0.264	0.059	0.146	0.383
PY duty cycle	0.348	0.054	0.240	0.456
Phase gap PD end to LP start	0.148	0.065	0.018	0.278
Phase gap LP end to PY start	–0.040	0.034	–0.108	0.029
LP start phase	0.533	0.054	0.426	0.640
PY start phase	0.758	0.060	0.638	0.877

DISCUSSION

Functional network output from different circuits

The main result of our analysis of the database of over 20 million network models is that similar network outputs can be generated with a large variety of combinations of synaptic strengths and intrinsic neuronal properties. Even for a narrowly defined type of output, such as the pyloric rhythm with its triphasic burst pattern and highly selected salient features, most of the synapses can vary in strength by several orders of magnitude.

Neural networks are often able to generate distinct activity patterns under different modulatory conditions. The crustacean pyloric network generates many different output patterns as a result of the application of a variety of modulators[11]. Requiring the functional model networks identified in this study to perform adequately under the influence of a variety of neuromodulator-induced changes in intrinsic and synaptic properties could potentially further constrain the number of functional model networks and the ranges of intrinsic and synaptic parameters they cover.

That similar functional network performance can be achieved with many different sets of network parameters suggests that it may not be necessary to fine-tune every synaptic or cellular parameter in a network to obtain the desired circuit output as long as there is an appropriate set of well-balanced network parameters. Taken at face value, these results allow us to make the following predictions: (i) the network outputs measured in different animals may differ less than some of the parameters of the underlying networks; (ii) network function may not require that each conductance or each synaptic strength be tightly specified, though some features of neural circuits may be genetically specified and others may be tuned by activity-dependent processes; (iii) network output depends on the correlated values of multiple synaptic and intrinsic conductances; and (iv) numerous compensations for altered values of some conductances or synaptic strengths may occur, so that some mutations may have little phenotypic effect owing to compensatory changes in other network values. Regulatory mechanisms consistent with these predictions have been demonstrated in different neural

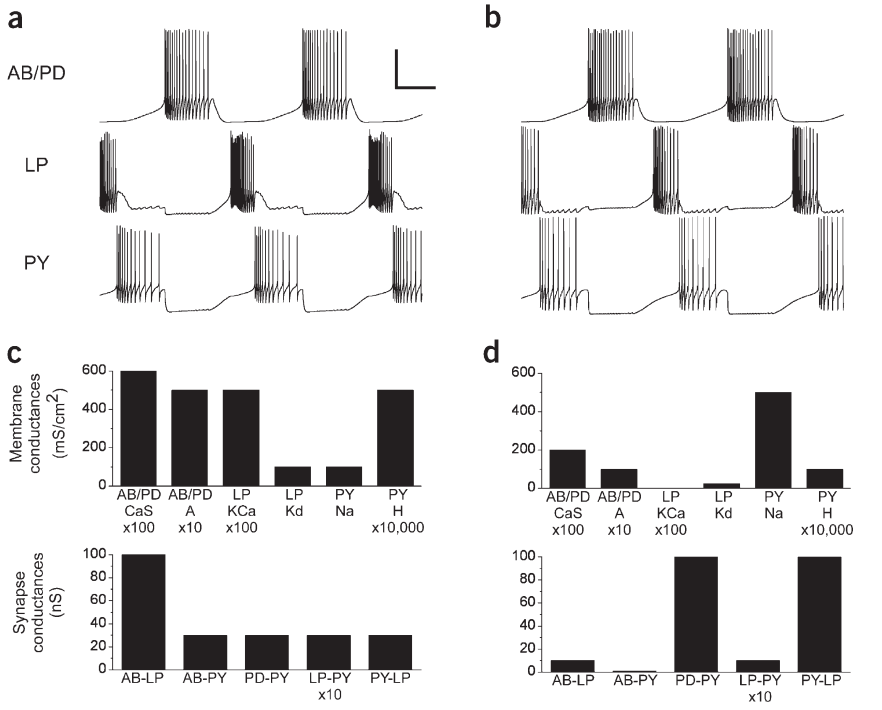

Figure 5 Similar model-network activity from different network properties. (**a**,**b**) Voltage traces from two model pyloric networks. Scale bars, 0.5 s and 50 mV. (**c**) Selected membrane conductances (top) and synaptic conductances of the model network shown in **a**. (**d**) Selected membrane conductances (top) and synaptic conductances of the model network shown in **b**. The two networks generated very similar activity in spite of widely differing cellular and synaptic properties.

systems, including activity-dependent[5,6,11] and activity-independent[10] regulation of membrane conductances in the crustacean pyloric system; conductance modulation in crayfish[20], *Drosophila*[21] and mouse[22] neurons by electrical activity; and activity-dependent regulation of excitatory[23,24] and inhibitory[25] synaptic properties in rat cortical circuits.

The possibility that similar network output may result from substantially different underlying mechanisms, which in turn could arise from activity-dependent and other tuning mechanisms, immediately gives rise to a number of questions. Although there are numerous indications in both the experimental and theoretical literature that intrinsic membrane currents[7,8,21,26–31] and synaptic strengths[32–36] may be homeostatically regulated, the regulatory processes observed in those studies are thought to occur at the level of a single neuron or synapse. In contrast, our study suggests that network performance, not individual neuronal activity or synaptic strength, might be the regulated property. For an animal, it is presumably far more important that its behavior be appropriately regulated than that any given intrinsic or synaptic parameter have a specific value. But if network performance is the locus of homeostatic and developmental regulation, this raises a series of questions: (i) Can stable network performance arise from local stability rules that set the properties of single-neuron excitability and/or synaptic strength? (ii) If local rules are not sufficient to maintain stable network output, are there monitors of network performance, such as sensory feedback from the target muscles, that are used developmentally to tune network output?

Comparison of the pyloric model networks to biological data

The main purpose of the simulations described here was to determine how tightly network parameters need to be regulated to produce a functional network output, not to study the pyloric network *per se*. However, the fact that the pyloric circuit has been well characterized experimentally allowed us to use experimental data to validate the pyloric model networks. Several properties of the model networks fit well with past experimental results. One is the relative strengths of the fast and slow synaptic connections from the AB/PD pacemaker to the LP and PY follower neurons. In pyloric model networks, the faster glutamatergic synapse to PY is equally likely to have any of the six maximal conductances tested in the database, whereas the slower cholinergic synapse from the AB/PD neuron to the PY neuron has a strong preference for high conductances (**Fig. 6c**, top row). In contrast, the connection from the AB/PD pacemaker neuron to the LP neuron tends to consist of a strong fast synapse and a weak slow synapse. These findings reproduce experimental results that suggest a strong glutamatergic and weak cholinergic synapse from AB/PD to LP, and *vice versa* for the AB/PD-to-PY connection[14,15]. This configuration of relative strengths of the fast and slow synapses from the pacemaker favors the pyloric burst order AB/PD-LP-PY because it allows LP to rebound faster than PY after inhibition from AB/PD.

The synapse from PY to LP is another example of agreement between the model-network outputs and experimental data. This synapse tends to be strong in the model pyloric networks (**Fig. 6c**, far right), consistent with the finding that this synapse is relatively strong in the biological pyloric circuit[19].

Some model pyloric networks contained synapses that had zero strength; these synapses may therefore appear to be redundant. However, seemingly redundant synapses in the pyloric circuit have been shown to stabilize periodic rhythm generation despite chaotic behavior of the neurons when isolated from the circuit. This is because an open network topology—in which at least one neuron receives no input from any of the other neurons—can generate a periodic rhythm only if none of the neurons in the circuit is chaotic[37]. The component neurons used here were all periodic in isolation, but it is conceivable that some of the open network configurations that generated pyloric rhythms in our simulations would not have done so if we had included chaotic neurons in our model-neuron pools.

Global implications

Although the pyloric rhythm of the crustacean stomatogastric nervous system was the specific example used here, we draw a general conclusion: that even tightly regulated network behavior can result from widely disparate sets of parameters in the processes that give rise to this behavior. This conclusion is relevant not only to the nervous system, but also to biochemical and signaling networks[38–42], as parallel and interacting pathways also occur in these networks. It may be possible for any given network parameter to be highly variable in different cells or in different individuals, as long as an appropriate set of compensating changes has occurred. The challenge for future work will be to uncover not only the structure of the networks, but how a target level of network performance is encoded and maintained.

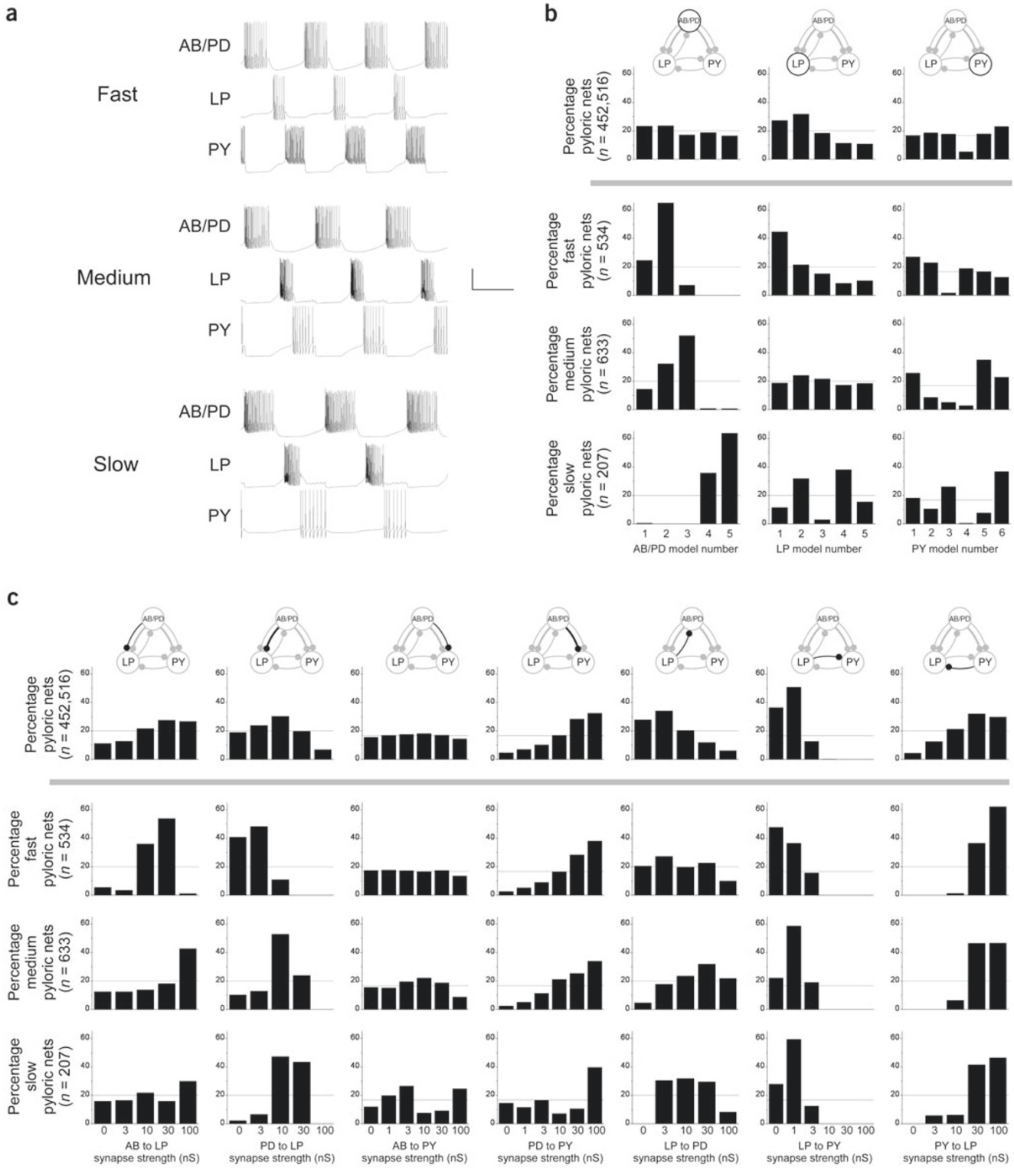

Figure 6 Cellular and synaptic properties of pyloric networks. (**a**) Voltage traces from pyloric networks in the fast, medium and slow burst-frequency ranges. Scale bars, 1 s and 50 mV. (**b**) Percentages of pyloric networks that contain a given AB/PD model neuron (left), LP model neuron (middle), or PY model neuron (right). Top row, distributions for all pyloric networks; bottom rows, distributions for fast, medium and slow pyloric networks. (**c**) Percentages of pyloric networks with a given synapse strength for each of the seven synapses in the network. Rows as in **b**. All horizontal lines, percentage expected for equal distribution over all cells or synaptic conductances. Synapse strengths in pyloric networks vary over wide ranges, even for pyloric networks in narrow frequency ranges.

METHODS

Model neurons. The model neurons used in the networks came from pools of five AB/PD models, five LP models and six PY models. The pools were selected from an existing database of single-compartment STG model neurons that have been described in detail[4] (this is referred to as "STG model-neuron database" throughout to avoid confusion with the network database described here). The model neurons feature a Na^+ current, I_{Na}; a fast and a slow transient Ca^{2+} current, I_{CaT} and I_{CaS}; a transient K^+ current, I_A; a Ca^{2+}-dependent K^+ current, $I_{K(Ca)}$; a delayed rectifier K^+ current, I_{Kd}; a hyperpolarization-activated inward current, I_H; and a leak current, I_{leak}. The voltage dependence and dynamics of the currents are based on recordings from lobster STG neurons[6] and are identical for all model neurons[4]. The maximal conductance of each current in each of the 16 model neurons used here is listed in **Table 2**. The model neurons were selected from the STG model-neuron database using the following criteria.

AB/PD models were intended to mimic the isolated pyloric pacemaker kernel in the crustacean STG. To find appropriate models, we searched the STG model-neuron database for bursting neurons with burst periods of 1–2 s, burst durations of 0.5–0.75 s, duty cycles of 0.3–0.4, and phase-response curves and slow-wave amplitudes similar to those of the biological pacemaker kernel. The entire selection process (which has been described in detail[4]) yielded nine model pacemakers that fit all the criteria. From these nine, we selected a pool of five AB/PD models in such a way as to cover as wide a range of intrinsic properties as possible. The intrinsic burst periods of the five pacemaker models were: AB/PD #1, 1.46 s; AB/PD #2, 1.49 s; AB/PD # 3, 1.58 s; AB/PD # 4, 1.61 s; AB/PD # 5, 1.64 s.

To identify suitable models for the follower LP and PY cells, we started by examining all models within the STG model-neuron database that were silent and slowly (<11.5 Hz) spiking, because both properties have been observed in synaptically isolated LP and PY neurons[43–46]. The silent models were then restricted to those with resting potentials between –60 mV and –50 mV[46]. Spiking models were excluded if their most hyperpolarized voltage value was below –70 mV, to ensure that model synaptic inputs with a reversal potential of –70 mV were hyperpolarizing at all times.

A crucial requirement for proper function of the follower neurons in the circuit was that they exhibit rebound bursts after inhibition from the pacemaker. To assess their rebound properties, we simulated a weak and a strong inhibitory synaptic input in all LP- and PY-model candidates. Both the weak and the strong stimulus consisted of a synaptic input with a burst from one of the five selected AB/PD models as the presynaptic waveform (see below for a description of the synapse model). For the weak stimulus, the connection from AB/PD to the follower neuron consisted of only a glutamatergic synapse with a maximal conductance of 10 nS. For the strong stimulus, the connection had both a glutamatergic and a cholinergic synapse with maximal conductances of 100 nS each. Follower-neuron candidate models were required to exhibit a rebound after both the weak and the strong stimulus, with at least five spikes in a burst lasting at least 200 ms before the first post-stimulus interspike interval longer than 100 ms.

Up to this point, the selection criteria were the same for LP and PY models. The two follower neuron types were distinguished by the delay between the end of the weak inhibitory stimulus and the first rebound spike[14]. LP models were required to have delays below 250 ms, whereas PY models were required to have delays between 300 and 500 ms. From the remaining 31 LP candidates and 57 PY candidates, we selected pools of five LPs and six PYs to cover a wide range of rebound delays and intrinsic properties (**Fig. 2**).

Model synapses. All synapses were simulated according to a standard model of synaptic dynamics[47]. The synaptic current is calculated as $I_s = g_s\, s(V_{post} - E_s)$, where g_s is the maximal synapse conductance or synapse strength, V_{post} is the membrane potential of the postsynaptic neuron and E_s is the reversal potential of the synapse. The activation variable s is governed by

$$\frac{ds}{dt} = \frac{\bar{s}(V_{pre}) - s}{\tau_s}$$

with

$$\bar{s}(V_{pre}) = \frac{1}{1 + \exp((V_{th} - V_{pre})/\Delta)} \quad \text{and} \quad \tau_s = \frac{1 - \bar{s}(V_{pre})}{k_-}$$

where V_{pre} is the membrane potential of the presynaptic neuron, V_{th} is the half-activation voltage of the synapse, Δ determines the slope of the activation curve and k_- is the rate constant for transmitter-receptor dissociation rate.

We modeled two types of synapses, because AB, LP and PY are glutamatergic neurons, whereas PD is cholinergic[16,48,49]. For glutamatergic synapses we set E_s at –70 mV and k_- at 1/40 ms, and for cholinergic synapses we set E_s at –80 mV and k_- at 1/100 ms. For both synapse types, we set V_{th} at –35 mV and Δ at 5 mV. These parameters approximately reproduced the slow time course of cholinergic IPSPs and the faster time course of glutamatergic IPSPs[15].

Network simulation and classification. Before a network was simulated, each individual neuron was initialized to a point on its isolated limit cycle that had been saved during the construction of the STG model-neuron database[4]. Synapses were initialized to a fully deactivated state. To allow the circuit to reach a new limit cycle and the initial state to decay, network activity was then simulated for 3 s without detection of spikes or any attempt at classification. Next, network activity was simulated and spikes were detected in epochs of 1 s. To classify the activity of a network, the detected spikes were analyzed, repetitive bursts were detected, and the burst period was determined for each neuron individually. Classification was attempted after each epoch, and the simulation was terminated as soon as the circuit was successfully classified.

Simulation implementation. Network simulation was implemented in a C++ program and executed on a varying number of 1.2-GHz processors in a Beowulf cluster (Dell). Numerical equations were integrated with an exponential Euler method[50]. The simulation and classification of all networks took several months and generated approximately 4 GB of output data.

Table 2 Maximal conductance densities of model neurons

Model	Maximal membrane conductance density in mS/cm^2							
neuron	g(I_{Na})	g(I_{CaT})	g(I_{CaS})	g(I_A)	g($I_{K(Ca)}$)	g(I_{Kd})	g(I_H)	g(I_{leak})
AB/PD 1	400	2.5	6	50	10	100	0.01	0.00
AB/PD 2	100	2.5	6	50	5	100	0.01	0.00
AB/PD 3	200	2.5	4	50	5	50	0.01	0.00
AB/PD 4	200	5.0	4	40	5	125	0.01	0.00
AB/PD 5	300	2.5	2	10	5	125	0.01	0.00
LP 1	100	0.0	8	40	5	75	0.05	0.02
LP 2	100	0.0	6	30	5	50	0.05	0.02
LP 3	100	0.0	10	50	5	100	0.00	0.03
LP 4	100	0.0	4	20	0	25	0.05	0.03
LP 5	100	0.0	6	30	0	50	0.03	0.02
PY 1	100	2.5	2	50	0	125	0.05	0.01
PY 2	200	7.5	0	50	0	75	0.05	0.00
PY 3	200	10.0	0	50	0	100	0.03	0.00
PY 4	400	2.5	2	50	0	75	0.05	0.00
PY 5	500	2.5	2	40	0	125	0.01	0.03
PY 6	500	2.5	2	40	0	125	0.00	0.02

ACKNOWLEDGMENTS

We thank L.F. Abbott for comments on an earlier version of this manuscript. This work was supported by a grant from the National Institute of Mental Health to E.M. (MH-46742), and by the Sloan-Swartz Center for Theoretical Neurobiology at Brandeis University.

COMPETING INTERESTS STATEMENT
The authors declare that they have no competing financial interests.

Received 26 August; accepted 28 September 2004
Published online at http://www.nature.com/natureneuroscience/

1. Foster, W.R., Ungar, L.H. & Schwaber, J.S. Significance of conductances in Hodgkin-Huxley models. *J. Neurophysiol.* **70**, 2502–2518 (1993).
2. Golowasch, J., Goldman, M.S., Abbott, L.F. & Marder, E. Failure of averaging in the construction of a conductance-based neuron model. *J. Neurophysiol.* **87**, 1129–1131 (2002).
3. Goldman, M.S., Golowasch, J., Marder, E. & Abbott, L.F. Global structure, robustness, and modulation of neuronal models. *J. Neurosci.* **21**, 5229–5238 (2001).
4. Prinz, A.A., Billimoria, C.P. & Marder, E. Alternative to hand-tuning conductance-based models: construction and analysis of databases of model neurons. *J. Neurophysiol.* **90**, 3998–4015 (2003).
5. Golowasch, J., Abbott, L.F. & Marder, E. Activity-dependent regulation of potassium currents in an identified neuron of the stomatogastric ganglion of the crab *Cancer borealis*. *J. Neurosci.* **19**, RC33 (1999).
6. Turrigiano, G.G., LeMasson, G. & Marder, E. Selective regulation of current densities underlies spontaneous changes in the activity of cultured neurons. *J. Neurosci.* **15**, 3640–3652 (1995).
7. Desai, N.S., Rutherford, L.C. & Turrigiano, G.G. Plasticity in the intrinsic excitability of cortical pyramidal neurons. *Nat. Neurosci.* **2**, 515–520 (1999).
8. Stemmler, M. & Koch, C. How voltage-dependent conductances can adapt to maximize the information encoded by neuronal firing rate. *Nat. Neurosci.* **2**, 521–527 (1999).
9. Marder, E. & Prinz, A.A. Modeling stability in neuron and network function: the role of activity in homeostasis. *Bioessays* **24**, 1145–1154 (2002).
10. MacLean, J.N., Zhang, Y., Johnson, B.R. & Harris-Warrick, R.M. Activity-independent homeostasis in rhythmically active neurons. *Neuron* **37**, 109–120 (2003).
11. Harris-Warrick, R.M., Marder, E., Selverston, A.I. & Moulins, M. *Dynamic Biological Networks. The Stomatogastric Nervous System* (MIT Press, Cambridge, Massachusetts, USA, 1992).
12. Marder, E. & Thirumalai, V. Cellular, synaptic and network effects of neuromodulation. *Neural Netw.* **15**, 479–493 (2002).
13. Marder, E. & Bucher, D. Central pattern generators and the control of rhythmic movements. *Curr. Biol.* **11**, R986–R996 (2001).
14. Hartline, D.K. & Gassie, D.V., Jr. Pattern generation in the lobster (Panulirus) stomatogastric ganglion. I. Pyloric neuron kinetics and synaptic interactions. *Biol. Cybern.* **33**, 209–222 (1979).
15. Eisen, J.S. & Marder, E. Mechanisms underlying pattern generation in lobster stomatogastric ganglion as determined by selective inactivation of identified neurons. III. Synaptic connections of electrically coupled pyloric neurons. *J. Neurophysiol.* **48**, 1392–1415 (1982).
16. Marder, E. & Eisen, J.S. Transmitter identification of pyloric neurons: electrically coupled neurons use different neurotransmitters. *J. Neurophysiol.* **51**, 1345–1361 (1984).
17. Maynard, D.M. Simpler networks. *Ann. NY Acad. Sci.* **193**, 59–72 (1972).
18. Hartline, D.K., Gassie, D.V. & Sirchia, C.D. PY Cell Types in the Stomatogastric System of *Panulirus*. in *The Crustacean Stomatogastric System* (eds. Selverston, A.I. & Moulins, M.) 75–77 (Springer-Verlag, Berlin, 1987).
19. Miller, J.P. & Selverston, A.I. Mechanisms underlying pattern generation in lobster stomatogastric ganglion as determined by selective inactivation of identified neurons. IV. Network properties of pyloric system. *J. Neurophysiol.* **48**, 1416–1432 (1982).
20. Hong, S.J. & Lnenicka, G.A. Characterization of a P-type calcium current in a crayfish motoneuron and its selective modulation by impulse activity. *J. Neurophysiol.* **77**, 76–85 (1997).
21. Baines, R.A., Uhler, J.P., Thompson, A., Sweeney, S.T. & Bate, M. Altered electrical properties in *Drosophila* neurons developing without synaptic transmission. *J. Neurosci.* **21**, 1523–1531 (2001).
22. Li, M., Jia, M., Fields, R.D. & Nelson, P.G. Modulation of calcium currents by electrical activity. *J. Neurophysiol.* **76**, 2595–2607 (1996).
23. Leslie, K.R., Nelson, S.B. & Turrigiano, G.G. Postsynaptic depolarization scales quantal amplitude in cortical pyramidal neurons. *J. Neurosci.* **21**, RC170 (2001).
24. Watt, A.J., van Rossum, M.C.W., MacLeod, K.M., Nelson, S.B. & Turrigiano, G.G. Activity coregulates quantal AMPA and NMDA currents at neocortical synapses. *Neuron* **26**, 659–670 (2000).
25. Kilman, V., van Rossum, M.C.W. & Turrigiano, G.G. Activity deprivation reduces miniature IPSC amplitude by decreasing the number of postsynaptic $GABA_A$ receptors clustered at neocortical synapses. *J. Neurosci.* **22**, 1328–1337 (2002).
26. LeMasson, G., Marder, E. & Abbott, L.F. Activity-dependent regulation of conductances in model neurons. *Science* **259**, 1915–1917 (1993).
27. Liu, Z., Golowasch, J., Marder, E. & Abbott, L.F. A model neuron with activity-dependent conductances regulated by multiple calcium sensors. *J. Neurosci.* **18**, 2309–2320 (1998).
28. Abbott, L.F. & LeMasson, G. Analysis of neuron models with dynamically regulated conductances. *Neural Comput.* **5**, 823–842 (1993).
29. Bell, A.J. Self-Organization in Real Neurons: Anti-Hebb in 'Channel Space'? in *Advances in Neural Information Processing Systems* (eds. Moody, J., Hanson, S. & Lippmann, R.) 59–66 (Morgan Kaufmann, San Mateo, 1992).
30. Siegel, M., Marder, E. & Abbott, L.F. Activity-dependent current distributions in model neurons. *Proc. Natl Acad. Sci. USA* **91**, 11308–11312 (1994).
31. Thoby-Brisson, M. & Simmers, J. Long-term neuromodulatory regulation of a motor pattern-generating network: maintenance of synaptic efficacy and oscillatory properties. *J. Neurophysiol.* **88**, 2942–2953 (2002).
32. Turrigiano, G.G., Leslie, K.R., Desai, N.S., Rutherford, L.C. & Nelson, S.B. Activity-dependent scaling of quantal amplitude in neocortical neurons. *Nature* **391**, 892–896 (1998).
33. Turrigiano, G.G. & Nelson, S.B. Hebb and homeostasis in neuronal plasticity. *Curr. Opin. Neurobiol.* **10**, 358–364 (2000).
34. Turrigiano, G.G. & Nelson, S.B. Homeostatic plasticity in the developing nervous system. *Nat. Rev. Neurosci.* **5**, 97–107 (2004).
35. Davis, G.W. & Bezprozvanny, I. Maintaining the stability of neural function: a homeostatic hypothesis. *Annu. Rev. Physiol.* **63**, 847–869 (2001).
36. Pulver, S.R., Bucher, D., Simon, D.J. & Marder, E. Constant amplitude of postsynaptic responses for single presynaptic action potentials but not bursting input during growth of an identified neuromuscular junction in the lobster, *Homarus americanus*. *J. Neurobiol.*, published online 8 September 2004 (doi:10.1002/neu.20066).
37. Huerta, R., Varona, P., Rabinovich, M.I. & Abarbanel, H.D.I. Topology selection by chaotic neurons of a pyloric central pattern generator. *Biol. Cybern.* **84**, L1–L8 (2001).
38. Weng, G., Bhalla, U.S. & Iyengar, R. Complexity in biological signaling systems. *Science* **284**, 92–96 (1999).
39. Bhalla, U.S. & Iyengar, R. Robustness of the bistable behavior of a biological signaling feedback loop. *Chaos* **11**, 221–226 (2001).
40. Brezina, V., Orekhova, I.V. & Weiss, K.R. Functional uncoupling of linked neurotransmitter effects by combinatorial convergence. *Science* **273**, 806–810 (1996).
41. Mutalik, V.K., Singh, A.P., Edwards, J.S. & Venkatesh, K.V. Robust global sensitivity in multiple enzyme cascade systems explains how the downstream cascade structure may remain unaffected by cross-talk. *FEBS Lett.* **558**, 79–84 (2004).
42. Blüthgen, N. & Herzel, H. How robust are switches in intracellular signaling cascades? *J. Theor. Biol.* **225**, 293–300 (2003).
43. Selverston, A.I. & Miller, J.P. Mechanisms underlying pattern generation in the lobster stomatogastric ganglion as determined by selective inactivation of identified neurons. I. Pyloric neurons. *J. Neurophysiol.* **44**, 1102–1121 (1980).
44. Golowasch, J. & Marder, E. Ionic currents of the lateral pyloric neuron of the stomatogastric ganglion of the crab. *J. Neurophysiol.* **67**, 318–331 (1992).
45. Harris-Warrick, R.M., Coniglio, L.M., Barazangi, N., Guckenheimer, J. & Gueron, S. Dopamine modulation of transient potassium current evokes phase shifts in a central pattern generator network. *J. Neurosci.* **15**, 342–358 (1995).
46. Harris-Warrick, R.M., Coniglio, L.M., Levini, R.M., Gueron, S. & Guckenheimer, J. Dopamine modulation of two subthreshold currents produces phase shifts in activity of an identified motoneuron. *J. Neurophysiol.* **74**, 1404–1420 (1995).
47. Abbott, L.F. & Marder, E. Modeling Small Networks. in *Methods in Neuronal Modeling: From Ions to Networks* (eds. Koch, C. & Segev, I.) 361–410 (MIT Press, Cambridge, 1998).
48. Marder, E. Cholinergic motor neurones in the stomatogastric system of the lobster. *J. Physiol. (Lond.)* **257**, 63–86 (1976).
49. Selverston, A.I., Russell, D.F., Miller, J.P. & King, D.G. The stomatogastric nervous system: structure and function of a small neural network. *Prog. Neurobiol.* **7**, 215–290 (1976).
50. Dayan, P. & Abbott, L.F. *Theoretical Neuroscience* (MIT Press, Cambridge, Massachusetts, USA, 2001).